

On Bubble Growth and Droplet Decay in Cosmological Phase Transitions

H. Kurki-Suonio^{a,*} and M. Laine^{b,c,†}

^a*Research Institute for Theoretical Physics and* ^b*Department of Physics,*
P.O. Box 9, FIN-00014 University of Helsinki, Finland

^c*Institut für Theoretische Physik, Philosophenweg 16, D-69120 Heidelberg, Germany*

(December 1, 1995)

We study spherically symmetric bubble growth and droplet decay in first order cosmological phase transitions, using a numerical code including both the complete hydrodynamics of the problem and a phenomenological model for the microscopic entropy producing mechanism at the phase transition surface. The small-scale effects of finite wall width and surface tension are thus consistently incorporated. We verify the existence of the different hydrodynamical growth modes proposed recently and investigate the problem of a decaying quark droplet in the QCD phase transition. We find that the decaying droplet leaves behind no rarefaction wave, so that any baryon number inhomogeneity generated previously should survive the decay.

PACS numbers: 98.80.Cq, 47.75.+f, 95.30.Lz

I. INTRODUCTION

The cosmological quark-hadron (QCD) phase transition [1] took place when the age of the universe was $t \sim 10^{-5}$ s. The order of this transition remains undetermined. If it is of first order, it may take up appreciable time. Unless the latent heat is very small compared with the surface tension, the probable sequence of events is:

1. Supercooling of the quark-gluon plasma.
2. Nucleation of bubbles of the hadron gas.
3. Rapid growth of hadron bubbles by deflagration.
4. Coupling in of particles without strong interactions.
5. Collisions of bubbles with shocks from other bubbles, and reheating of the plasma to the critical temperature.
6. Slow growth of the hadron bubbles paced by the expansion of the universe, leading to percolation.
7. Slow shrinking of remaining regions of quark plasma and their becoming spherical.
8. Decoupling of particles without strong interactions.
9. Evaporation of the quark droplets.

The electroweak (EW) phase transition [2] took place earlier, at $t \sim 10^{-11}$ s. It is likely to be of first order, since there is baryon asymmetry in the universe [3]. However, within the Standard Model, the order remains unclear for Higgs masses $m_H \gtrsim 80$ GeV. If the transition is of

first order, it will likewise proceed through growing bubbles and shrinking droplets, although the details will be different. For instance, there may not be a stage of slow growth (6-7).

Clearly, to understand the possible physical consequences of the cosmological phase transitions, all the stages should be thoroughly understood. The nucleation period (1-2) from the critical temperature T_c to the nucleation temperature T_n seems to be rather well under control, and we do not touch it here. For the QCD phase transition, the present understanding of the other stages is the following: The general hydrodynamics of bubble growth has been studied extensively [4–16]. Hydrodynamics alone cannot determine the bubble solution, but due to the strong coupling constant, there is not very much more one can say [17,18]. The coupling in of electromagnetic radiation with the strongly interacting matter at about the scale 10^4 fm is discussed in [19,20], the collisions with shocks in [7,18], and the slow stages at T_c in [1]. In our opinion, the possible formation of a shrinking similarity solution [21] at stage (7) is not completely understood. Assuming that this happens, the decoupling of electromagnetic radiation at the scale 10^4 fm, and the final stages until the quark droplet has a radius of about 1 fm, have been discussed in [21,22]. One should note that depending on the values of the latent heat and surface tension, the phase transition might also proceed rather differently from the standard scenario assumed here [23].

In this paper, we complete the hydrodynamic study of growing bubbles (3) presented in [16], and investigate in detail the final stages (9) from a radius of about 200 fm until the time that the quark droplet has completely disappeared, thus improving on [21]. The final stages are important since they determine the baryon number inhomogeneity resulting from the QCD phase transition.

For the EW phase transition, there are a number of microscopic investigations of bubble growth [24–29]. These assume that the change of temperature across the phase transition surface, $\delta T/(T_c - T_n)$, is vanishing, and hence are applicable only for very weak deflagrations. A phenomenological investigation with one free parameter but without any limitations on $\delta T/(T_c - T_n)$ is in [18]. Recently there has appeared also a microscopic investigation with hydrodynamics included [30], so that stage (3) seems to be reasonably well under control. As to the later stages, in [15] it was argued that the collisions with the shock fronts (5) might have interesting effects, if the bubble walls are slowed down appreciably. This could happen

*Email: hkurkisu@pcu.helsinki.fi

†Email: m.laine@thphys.uni-heidelberg.de

if the temperature rises close to T_c . Based on simple perturbative estimates, one often assumes that reheating to T_c and the stages (6-7) do not exist; however, this need not necessarily be the case, see e.g. [31]. In particular, lattice simulations [32] suggest that the surface tension may be smaller than the perturbative value, leading to smaller supercooling and possibly to a reheating to T_c . Then the final stages would proceed similarly to the QCD case. The results of this paper are applicable to the general characteristics of bubble growth (3) and to the final stages (9).

We study the growth of bubbles and the decay of droplets in first-order phase transitions as a hydrodynamical problem. We shall use the quark/hadron terminology, but as stated, our results are qualitative and apply to some extent also to the electroweak phase transition. A major uncertainty in these studies is the phase boundary, the bubble or droplet wall, which remains poorly understood, especially for QCD. Hence one usually has to resort to some kind of parametrization of its properties. We use a cosmic-fluid-order-parameter-field model, which allows simultaneous treatment of the phase boundary and surrounding hydrodynamics within a single framework [18]. We have written a hydrodynamical code using this model; an earlier version was plane-symmetric, but we now have a spherically symmetric version. In the next Section, we describe the model and how it differs from the one in [21,22]. In Section III we investigate bubble growth with our model, and in Section IV droplet decay.

II. THE MODEL

We summarize here our cosmic-fluid-order-parameter-field model [18]. We ignore the chemical potential related to the small baryon number. The local state of matter is then described by three quantities: a local temperature T , a local flow velocity u^μ and a local value for the order parameter ϕ . The order parameter has a temperature-dependent effective potential $V(\phi, T)$. The (meta)stable states of the system are defined by the minima of the effective potential.

The equation of state is

$$\epsilon(\phi, T) = 3aT^4 + V(\phi, T) - T \frac{\partial V}{\partial T}, \quad (1)$$

$$p(\phi, T) = aT^4 - V(\phi, T). \quad (2)$$

where $a = (\pi^2/90)g_*$. The energy-momentum tensor is

$$T^{\mu\nu} = \partial^\mu \phi \partial^\nu \phi - g^{\mu\nu} \left(\frac{1}{2} \partial_\alpha \phi \partial^\alpha \phi \right) + w u^\mu u^\nu + g^{\mu\nu} p, \quad (3)$$

where $w \equiv \epsilon + p$ and the metric convention is $(-+++)$. The energy-momentum conservation equation $T_{;\mu}^{\mu\nu} = 0$ is split into two parts:

$$T_{;\mu}^{\mu\nu}(\text{field}) = \phi_{;\mu}^{\mu} \phi^{\nu} - \frac{\partial V}{\partial \phi} \phi^{\nu} = \eta u^\mu \phi_{,\mu} \phi^{\nu}, \quad (4)$$

$$T_{;\mu}^{\mu\nu}(\text{fluid}) = (w u^\mu u^\nu)_{;\mu} + p^{\nu} + \frac{\partial V}{\partial \phi} \phi^{\nu} = -\eta u^\mu \phi_{,\mu} \phi^{\nu}, \quad (5)$$

where “;” is a covariant derivative. Here η is a dissipative constant relating entropy production to the gradients of ϕ through $T(su^\mu)_{;\mu} = \eta(u^\mu \phi_{,\mu})^2$. Eq. (4) contains the equation for the ϕ -field,

$$\phi_{;\mu}^{\mu} - \frac{\partial V}{\partial \phi} = \eta u^\mu \phi_{,\mu}. \quad (6)$$

Eq. (6) (or its equivalent) could in principle be derived from field theory at least for the EW case, see e.g. [30], but we do not here attempt to do so.

In the spherically symmetric case, eq. (5) contains two independent equations. For numerical hydrodynamics it is best to choose eq. (5) with $\nu = r$, together with the contraction of eq. (5) with u_ν :

$$(\epsilon u^\mu)_{;\mu} + p u_{;\mu}^\mu - \frac{\partial V}{\partial \phi} u^\mu \phi_{,\mu} = \eta (u^\mu \phi_{,\mu})^2. \quad (7)$$

From eqs. (5), (6), (7), the final spherically symmetric equations in Minkowski space then become

$$-\partial_t^2 \phi + \frac{1}{r^2} \partial_r (r^2 \partial_r \phi) - \frac{\partial V}{\partial \phi} = \eta \gamma (\partial_t \phi + v \partial_r \phi), \quad (8)$$

$$\begin{aligned} \partial_t E + \frac{1}{r^2} \partial_r (r^2 E v) + p \left[\partial_t \gamma + \frac{1}{r^2} \partial_r (r^2 \gamma v) \right] \\ - \frac{\partial V}{\partial \phi} \gamma (\partial_t \phi + v \partial_r \phi) = \eta \gamma^2 (\partial_t \phi + v \partial_r \phi)^2, \end{aligned} \quad (9)$$

$$\begin{aligned} \partial_t Z + \frac{1}{r^2} \partial_r (r^2 Z v) + \partial_r p + \frac{\partial V}{\partial \phi} \partial_r \phi \\ = -\eta \gamma (\partial_t \phi + v \partial_r \phi) \partial_r \phi, \end{aligned} \quad (10)$$

where $E \equiv \epsilon \gamma$ and $Z \equiv w \gamma^2 v$.

For the effective potential $V(\phi, T)$ we use the simple parametrization

$$V(\phi, T) = \frac{1}{2} \gamma (T^2 - T_0^2) \phi^2 - \frac{1}{3} \alpha T \phi^3 + \frac{1}{4} \lambda \phi^4 \quad (11)$$

where [9,17]

$$T_0 = \frac{T_c}{\sqrt{1 + 6\sigma/(Ll_c)}}, \quad (12)$$

$$\alpha = \frac{1}{\sqrt{2\sigma l_c^5 T_c^2/3}}, \quad (13)$$

$$\gamma = \frac{L + 6\sigma/l_c}{6\sigma l_c T_c^2}, \quad (14)$$

$$\lambda = \frac{1}{3\sigma l_c^3}. \quad (15)$$

Here σ is the surface tension, l_c is the correlation length, L is the latent heat, and T_c is the critical temperature of the transition. We use the functional form in eq. (11) due

to its simplicity; our results are qualitative and we expect them to remain the same for any $V(\phi, T)$ including a first order phase transition.

Let us now compare our model with that used in [21,22] (RMP, RM) for studying droplet decay. The main difference is that in our model the phase transition surface has a microscopic structure and a finite width, whereas in [21,22] it is a discontinuity, across which explicit jump conditions are imposed. For this reason RMP have to stop the evolution of the decaying droplet at a radius of about 1 fm when the width of the interface starts to have significance, whereas we are able to follow the decay until the very end and beyond. We also believe that in our code the velocity determination by the coefficient η is more natural: we do not need to know anything about the structure of the solution beforehand; a fact which, for instance, allowed us to find new kinds of solutions in [16]. In [21,22], the velocity is fixed by giving the ratio of the hydrodynamical and thermal fluxes at the deflagration front.

On the other hand, the code in [21,22] contains features we do not have. First, RMP have an expanding background metric. We do not expect the extremely slow expansion to have any effect at the short time scales we are investigating. Second, in [22] the electromagnetic radiation is treated properly, allowing RM to investigate the decoupling of radiation from the strongly interacting matter at a radius of about 10^4 fm, which is important for concentrating baryon number inside the quark droplet. Here we study only the final stages when the bubble has a radius smaller than 200 fm, so that the decoupling has already taken place. Hence our number of degrees of freedom is that of the strongly interacting particles. We take the physical result of the decoupling period, namely a strongly increased baryon number density within a radius of $10^3 - 10^4$ fm around the droplet [22], as an initial condition for our analysis of droplet decay.

III. BUBBLE GROWTH MECHANISMS

In [16] we discussed the different hydrodynamical growth mechanisms of phase transition bubbles. We found three different classes: (1) weak deflagrations moving at a subsonic speed and preceded by a shock front and a compression wave; (2) Jouguet deflagrations moving at a supersonic speed, preceded by a shock front and a compression wave, and followed by a rarefaction wave; and (3) weak detonations moving at a supersonic speed, and followed by a rarefaction wave.

Note that for small supercooling, the condition of non-negative entropy production allows only weak deflagrations [5,9,23]. Moreover, adding information about the microscopic entropy producing mechanism, the solution becomes fixed; for instance, for the EW case mildly relativistic weak deflagrations seem probable [30]. The above three classes refer to a case when the entropy condition

does not forbid any of the solutions, and the parameter η is allowed to vary freely. At least for the QCD case, there is ample parameter space for all three kinds of solutions [23].

We set out to verify that all three classes can be realized. We choose parameter values which allow the three classes: $L = 0.1T_c^4$, $\sigma = 0.1T_c^3$, $l_c = 6T_c^{-1}$, $a = 34.25\pi^2/90$. The nucleation temperature corresponding to these is $T_{\text{init}} = 0.86T_c$ [23]. We start with initial data where there is a small “recently nucleated” bubble surrounded by homogeneous fluid at rest. The bubble will start to grow and we follow it until the configuration becomes self-similar, see Fig. 1.

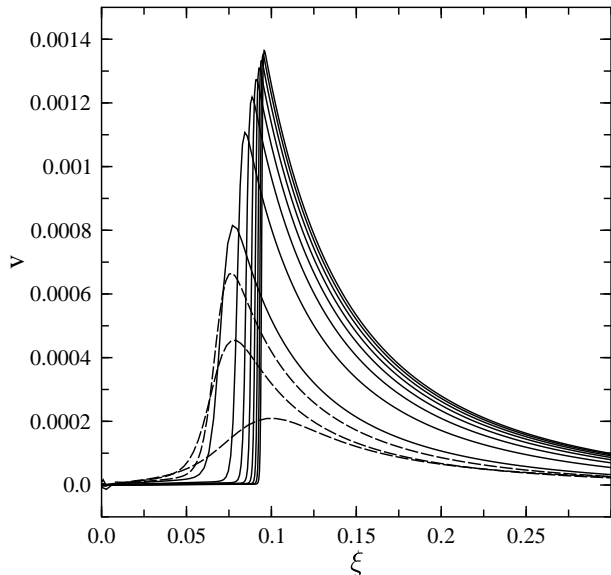


FIG. 1. The velocity profile approaches the similarity solution as the bubble grows. This run is for $\eta = 1.0T_c$. The time interval between the dashed curves is $\Delta t = 158.75T_c^{-1}$, and between the solid curves $\Delta t = 675T_c^{-1}$. The horizontal axis is $\xi \equiv r/t$, distance scaled with time.

The velocity of the bubble wall will depend on the dissipative constant η . We covered the range from $\eta = 0.01T_c$ to $\eta = 10T_c$, and found all three classes: (1) weak deflagrations for $\eta \gtrsim 0.13T_c$; (2) Jouguet deflagrations for $0.12T_c \lesssim \eta \lesssim 0.13T_c$; and (3) weak detonations for $\eta \lesssim 0.12T_c$. In Fig. 2 we show a sequence of final velocity profiles for a set of runs, and in Fig. 3 we show the wall and shock velocities as a function of η . The shock fronting the compression wave in the deflagration bubble solutions becomes exponentially weak for slowly growing bubbles, and we did not resolve the shock for $\eta \gtrsim 0.17T_c$. Fig. 4 shows an example from each solution class.

We see (Fig. 3) that as η is decreased the wall velocity grows smoothly until it is close to the speed of sound. Then the wall velocity appears to have some difficulty breaking the sound barrier. (In a Jouguet deflagration

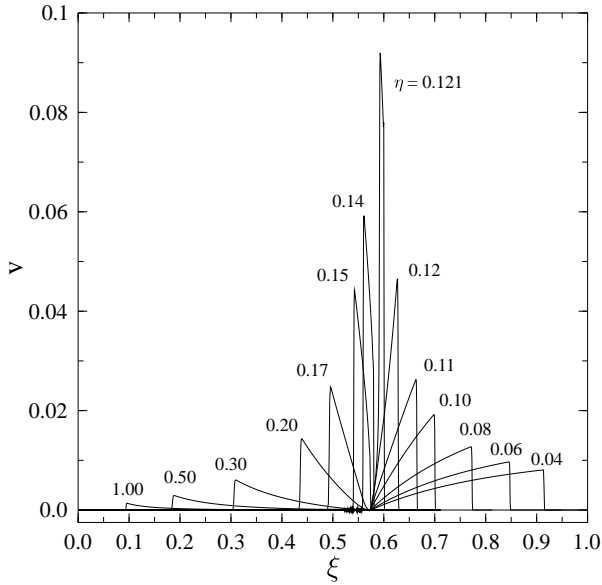


FIG. 2. A sequence of velocity profiles for bubbles with different values of η (given in units of T_c next to each profile). These profiles are from our hydrodynamical runs. Compare with Fig. 3 of [16], where the profiles are solutions of eqs. (20) and (21) (with a bag equation of state).

the wall is subsonic with respect to the fluid just ahead of the wall, and it is moving at the speed of sound with respect to the fluid just behind, although the velocity with respect to the bubble center, “the wall velocity”, already exceeds the speed of sound). The increase in wall velocity slows down, until at $\eta \sim 0.12T_c$ the solution shifts from a deflagration to a detonation solution and the wall velocity jumps abruptly. Thus we do not have solutions for wall velocities between $v = 0.593$ and $v = 0.635$.

In [16] we described similarity solutions for all wall velocities. The reason that we do not here find solutions in the above range $0.593 \dots 0.635$, is that there are pairs of solutions with different wall velocities corresponding to the same value of η . The slower one is a Jouguet deflagration, the faster one a weak detonation. Only one of these two is realized for a given initial configuration. Thus when the solution shifts from a deflagration to a detonation, there is a jump in wall velocity. In fact, in the runs with the fastest deflagrations, the bubble first went into a detonation configuration before settling into a deflagration, see Fig. 5.

IV. DROPLET DECAY

Kajantie and Kurki-Suonio (KK) [7] have discussed the shrinking quark droplet. There is an outward fluid flow from the surface of the droplet. When the droplet van-

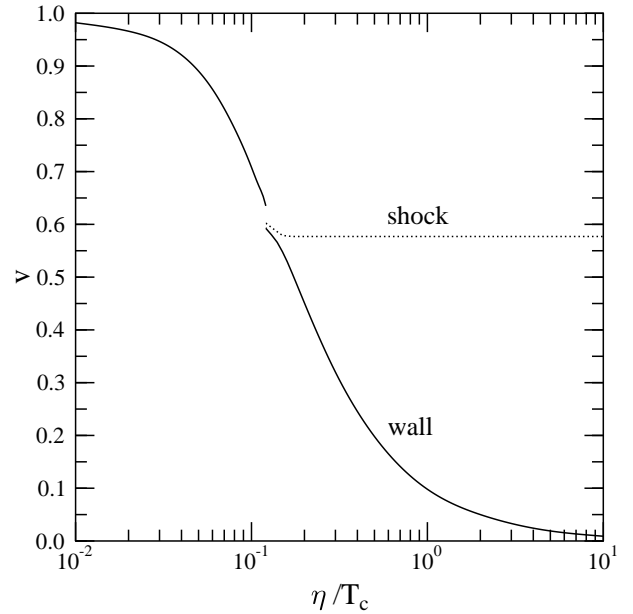


FIG. 3. The bubble wall velocity and the shock velocity as a function of η .

ishes the source of this flow disappears. This led KK to conclude that the evaporation site sends out a rarefaction wave by which the outward flow is stopped. KK did not consider the effect of surface tension on droplet evaporation.

Rezzolla, Miller, and Pantano [21] have improved upon the work of KK. They conclude that the flow pattern around a shrinking droplet settles into a similarity solution. If the similarity solution would hold till the end, the droplet would leave behind a homogeneous fluid at rest, since all structure around the droplet would have shrunk to zero size at the moment the droplet vanishes. But as the droplet becomes small, the surface tension causes the droplet wall to accelerate, and the droplet actually vanishes before the surrounding outward flow pattern. Apparently RMP have not followed the evolution past the droplet disappearance with their code. This we have done with ours.

We start with the similarity solution as an initial condition. Thus we need to construct this solution in our model. Let us first discuss the regions away from the phase transition surface, where the order parameter lies at the minima $\phi = 0$ and $\phi = \phi_{\min}(T)$ in the two phases ($\partial V/\partial\phi = 0$). We assume the distance scale is large enough so that $\partial_\mu\phi$ terms can be ignored in $T^{\mu\nu}$. Then we have

$$\epsilon_q(T) = 3aT^4, \quad (16)$$

$$p_q(T) = aT^4, \quad (17)$$

$$\epsilon_h(T) = 3aT^4 + V(\phi_{\min}(T), T) - T \frac{\partial V}{\partial T}(\phi_{\min}(T), T), \quad (18)$$

$$p_h(T) = aT^4 - V(\phi_{\min}(T), T). \quad (19)$$

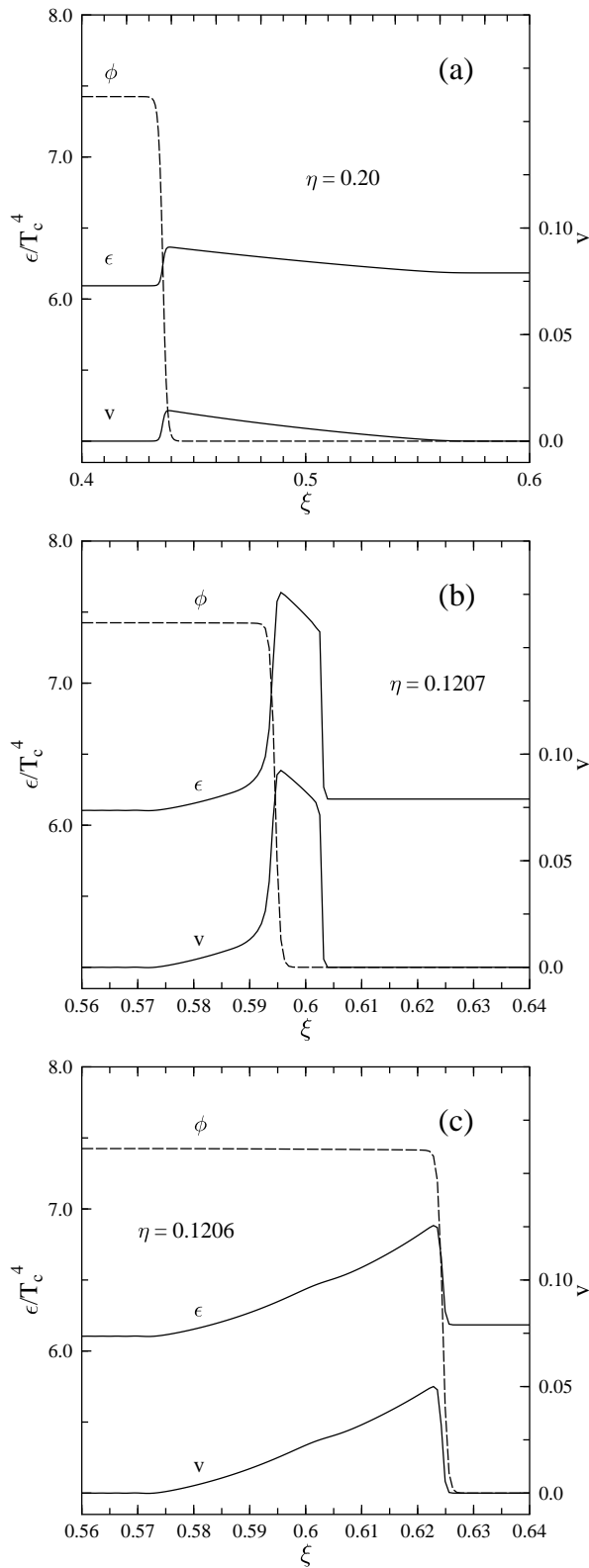


FIG. 4. The energy density, velocity, and order parameter profiles for the three different solution classes. The first (a) is a weak deflagration, the second (b) a Jouguet deflagration, and the third (c) a weak detonation.

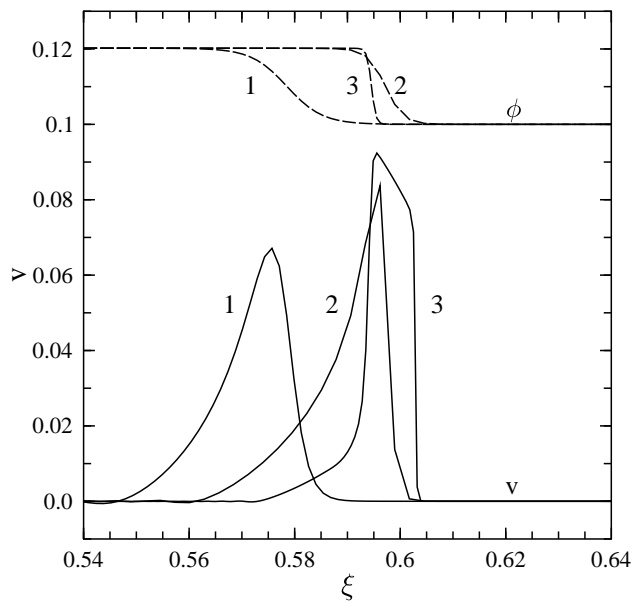


FIG. 5. A bubble ($\eta = 0.1207T_c$) which first goes to a detonation configuration before settling to a deflagration. The three profiles are from times $t_1 = 1350T_c^{-1}$, $t_2 = 2700T_c^{-1}$, and $t_3 = 10800T_c^{-1}$.

The similarity solution depends on the coordinates r and t only through the combination $\xi \equiv r/t$. For a shrinking solution, we must choose $t = 0$ at the moment of disappearance, so $t < 0$ and thus $\xi < 0$. The similarity solution has homogeneous fluid at rest inside the droplet, $v = 0$, $\epsilon = \epsilon_q(T_q)$. The droplet surface at $\xi = \xi_{\text{defl}}$ is a deflagration front, the phase boundary moving in at a speed $|\xi_{\text{defl}}|$. The usual deflagration conditions give us then the fluid state just outside the droplet wall, with fluid flowing outwards. The profile $\epsilon(\xi)$, $v(\xi)$ of this compression wave is solved from [4,6]

$$\left[\frac{1}{c_s^2(T)}(v - \xi)^2 - (1 - v\xi)^2 \right] \frac{dv}{d\xi} = 2\frac{v}{\xi}(1 - v\xi)(1 - v^2), \quad (20)$$

$$\frac{1}{\epsilon(T) + p(T)} \frac{dp}{dT}(T) \frac{dT}{d\xi} = \frac{\xi - v}{1 - v\xi} \frac{1}{1 - v^2} \frac{dv}{d\xi}. \quad (21)$$

The velocity is positive (outwards) and becomes zero at the sonic point $\xi = -c_s$, where we have a weak discontinuity. For $|\xi| > c_s$ the fluid is at rest with constant energy density. (Note that there is no shock front, unlike in the case of an expanding deflagration bubble). In Fig. 6 we show a similarity solution for the case $T_q = 0.99$, $\xi_{\text{defl}} = -0.05$.

For the phase transition surface we use a finite-width wall obtained with our stationary plane-symmetric code [18]. This gives the initial data for our dynamical code.

We present results from a run with parameter values $L = 4T_c^4$, $\sigma = 0.5T_c^3$, $l_c = 1T_c^{-1}$, and $a = 40\pi^2/90$, using

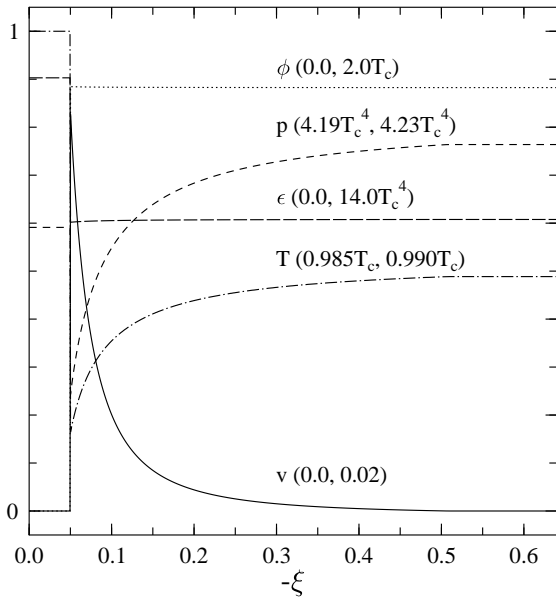


FIG. 6. A similarity solution for a shrinking droplet. The two values in the brackets refer to the value of the corresponding quantity at “0” and “1” of the y -axis.

an initial condition with $T_q = 0.99T_c$. (This is a fairly arbitrary choice, as there is large uncertainty about the values of these parameters, and we are thus looking for qualitative features only). The initial data is the similarity solution for the case $v_{\text{defl}} = -0.05$, and we set the initial radius of the droplet to be $r = 200T_c^{-1}$ (for QCD T_c^{-1} is just 1 fm, and for the EW case 10^{-3} fm). Now the actual wall velocity will depend on the dissipation parameter η . The value of η corresponding to a given v_{defl} can be found by trying out different values. Because of the fairly small initial size, there are already some small-scale effects and the solution should be deviating somewhat from the similarity solution. Therefore using the similarity solution as initial data will cause some disturbance to spread out from the wall to alter the profile. We minimized this initial disturbance by choosing $\eta = 1.97T_c$, giving an actual initial wall velocity $v_{\text{defl}} = -0.047$.

Figs. 7–10 show results from this run. At first we stay fairly close to the similarity solution but as the droplet gets smaller the wall is accelerated inwards, and the temperature and energy density rise inside the droplet. As the droplet disappears the outward flow leads to an underdense region with lower temperature in the center. The fluid flow then turns around filling this underdense region. A pulse of inward flow is thus sent outwards, and decays rapidly. The end result is homogeneous fluid at rest. Thus we see no rarefaction wave propagating to infinity after the decay. This is in contrast to expectations in [7,21,22].

In Fig. 9 we show the compression factor ρ (density of noninteracting test particles moving with the fluid). In

the end the thermodynamical properties (T, v, ϕ) of the fluid become homogeneous. There is a small depression in the final ρ at the droplet evaporation site. This is due to the droplet surface energy which was converted into thermal energy. Because of this extra energy some decompression was needed to even out the energy density.

Note that due to the difficulty of getting baryon number through the wall, the baryon number tends to concentrate on the inside of the droplet surface, and is thus not moving with the fluid [1,33–37,22]. Thus the compression factor ρ does not represent baryon number density. However, it can be viewed as representing a background motion of the baryon number, upon which the baryon-number-concentrating effects are superimposed. Thus we see that the hydrodynamical flow itself does not lead to any inhomogeneity in the baryon number, except the tiny depression at the droplet evaporation site.

RM [22] studied the effect of radiative energy transfer out of the quark droplet on the baryon number distribution. We are studying scales where this transfer has ceased to operate as the droplet has become transparent to radiation. Thus we can combine our work with RM by considering their result at the relevant time as an initial condition for our runs. Their compression factor ρ_{RM} can be viewed as being proportional to baryon number density in an idealization where other baryon number concentrating effects are ignored. Let us do this idealization in the discussion below. RM found that the shrinking droplet leaves behind a region with a high overdensity in baryon number, whose radius is of the order of the mean free path $\lambda \sim 10^4 \text{fm}$ of the electromagnetic radiation. Inside the quark droplet there is an even higher baryon number density. As we are considering the region $r \ll \lambda$, we can take our compression factor ρ to denote the baryon number density normalized to the value it has in the end at about $r \sim 10^2 \text{fm}$, where it is fairly homogeneous. Thus our Fig. 9(a) shows the baryon number density contrast between the quark and hadron phases (the numerical value is much smaller in our case than in [22] because of different parameter values used). There are two contributions to this density contrast: (1) the decompression due to the change in equation of state as the fluid passes through the phase boundary, and (2) the extra overdensity inside the droplet due to surface tension, which becomes significant in the end. There will be no remnant of this higher density inside the droplet after the droplet has disappeared (in reality, there probably will be a remnant due to effects we are ignoring here [35]). Contribution (1) is eliminated as the fluid is converted to the hadron phase. Contribution (2) is eliminated as the thermodynamical variables are evened out by the outward pulse (see Fig. 8). Thus the ρ_{RM} outside the droplet represents the final baryon number distribution, and it is not disturbed by any rarefaction wave. For $r \ll \lambda$ the baryon number density is homogeneous except for the central small depression caused by the released droplet surface energy (see Fig. 9(b)). The baryon number overdensity within $r \lesssim 10^4 \text{fm}$ is later eliminated

mainly by neutron diffusion [38].

V. CONCLUSIONS

We have studied the growth of bubbles and decay of droplets in cosmological phase transitions using a spherically symmetric version of our hydrodynamic code based on a cosmic-fluid–order-parameter model [18] of the transition.

We demonstrate how an initial small newly nucleated bubble begins to grow and evolves to a similarity solution. The wall velocity depends on the dissipative constant η . We find all three classes of hydrodynamic similarity solutions: weak deflagrations, Jouguet deflagrations, and weak detonations. In the first class the wall velocity is subsonic, in the other two classes supersonic with respect to the origin.

Not all wall velocities are realized as the value of η is varied. For a certain range in η , there would be both a Jouguet deflagration and a weak detonation solution with the same value of η , but a different wall velocity. As the solution shifts from the former class to the latter, there is thus a jump in wall velocity.

Note that all classes of solutions are not possible for all values of the other parameters [5,9,23]. Typically weak deflagrations are always possible, but detonations and Jouguet deflagrations may not be reached; or the solution may shift directly from weak deflagrations to weak detonations as η is decreased, skipping the class of Jouguet deflagrations [23].

We followed the evaporation of a quark droplet starting from a similarity solution. The droplet deviates from the similarity solution in the end when small-scale effects from the surface tension and finite wall thickness become significant. The nature of the fluid flow after the droplet evaporation differs from what has been previously suggested [7,21,22]. The deviation from similarity flow in the end leads to a temporary energy overdensity at the evaporation site, surrounded by a shell of underdensity. This inhomogeneity is eliminated by an outward moving pulse which decays rapidly. This effect does not extend beyond the small scales where the droplet deviated from the similarity solution.

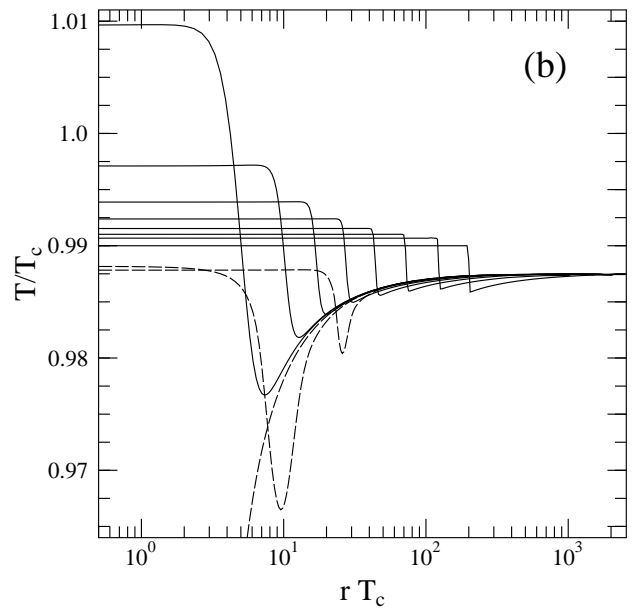
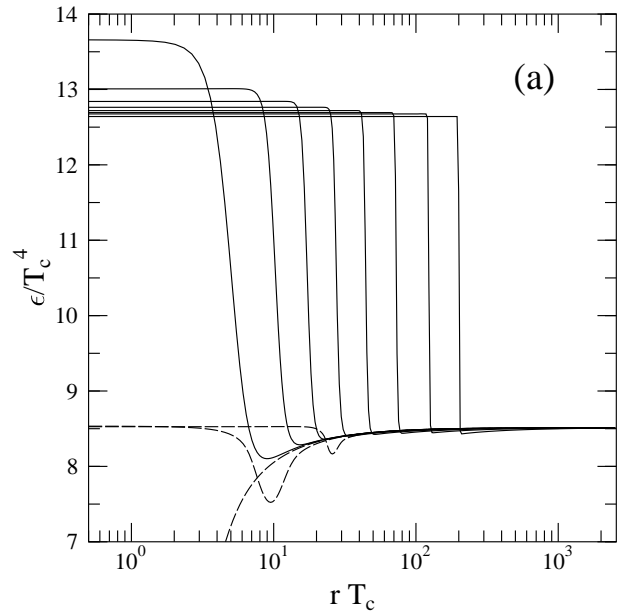
Our model does not contain the effects which concentrate baryon number: the suppression of baryon flow through the wall and the radiative entropy transfer out of the droplet [1,33–36,22]. The temporary hydrodynamic compression at the final stage of droplet decay does not affect the baryon/entropy ratio and thus has no lasting effect on the baryon density. There is a small decompression at the very center to accommodate the droplet surface energy which has been converted to thermal energy. The absence of a global rarefaction wave indicates that any previously generated baryon number inhomogeneity at the scale 10^4 fm is not diluted away by the hydrodynamics related to droplet decay.

ACKNOWLEDGEMENTS

We are grateful to the Center for Scientific Computing (Finland) for computational resources.

-
- [1] E. Witten, Phys. Rev. D 30 (1984) 272, and references therein.
 - [2] D.A. Kirzhnits, JETP Lett. 15 (1972) 529; D.A. Kirzhnits and A.D. Linde, Phys. Lett. B 42 (1972) 471.
 - [3] V.A. Kuzmin, V.A. Rubakov, and M.E. Shaposhnikov, Phys. Lett. B 155 (1985) 36; M.E. Shaposhnikov, Nucl. Phys. B 287 (1987) 757.
 - [4] P.J. Steinhardt, Phys. Rev. D 25 (1982) 2074.
 - [5] M. Gyulassy, K. Kajantie, H. Kurki-Suonio, and L. McLerran, Nucl. Phys. B 237 (1984) 477.
 - [6] H. Kurki-Suonio, Nucl. Phys. B 255 (1985) 231.
 - [7] K. Kajantie and H. Kurki-Suonio, Phys. Rev. D 34 (1986) 1719.
 - [8] J.C. Miller and O. Pantano, Phys. Rev. D 40 (1989) 1789, D 42 (1990) 3334.
 - [9] K. Enqvist, J. Ignatius, K. Kajantie, and K. Rummukainen, Phys. Rev. D 45 (1992) 3415.
 - [10] B. Link, Phys. Rev. Lett. 68 (1992) 2425.
 - [11] S.A. Bonometto and O. Pantano, Phys. Rep. 228 (1993) 175.
 - [12] P. Huet, K. Kajantie, R.G. Leigh, B.-H. Liu, and L. McLerran, Phys. Rev. D 48 (1993) 2477.
 - [13] M. Kamionkowski, A. Kosowsky, and M.S. Turner, Phys. Rev. D 49 (1994) 2837.
 - [14] M. Laine, Phys. Rev. D 49 (1994) 3847.
 - [15] A.F. Heckler, Phys. Rev. D 51 (1995) 405.
 - [16] H. Kurki-Suonio and M. Laine, Phys. Rev. D 51 (1995) 5431.
 - [17] K. Kajantie, Phys. Lett. B 285 (1992) 331.
 - [18] J. Ignatius, K. Kajantie, H. Kurki-Suonio, and M. Laine, Phys. Rev. D 49 (1994) 3854.
 - [19] L. Rezzolla and J.C. Miller, Class. Quantum Grav. 11 (1994) 1815.
 - [20] J.C. Miller and L. Rezzolla, Phys. Rev. D 51 (1995) 4017.
 - [21] L. Rezzolla, J.C. Miller, and O. Pantano, Phys. Rev. D 52 (1995) 3202.
 - [22] L. Rezzolla and J.C. Miller, SISSA 116/95/A [astro-ph/9510039].
 - [23] J. Ignatius, K. Kajantie, H. Kurki-Suonio, and M. Laine, Phys. Rev. D 50 (1994) 3738.
 - [24] N. Turok, Phys. Rev. Lett. 68 (1992) 1803.
 - [25] M. Dine, P. Huet, R.G. Leigh, A.D. Linde, and D. Linde, Phys. Rev. D 46 (1992) 550.
 - [26] B.-H. Liu, L. McLerran, and N. Turok, Phys. Rev. D 46 (1992) 2668.
 - [27] S.Yu. Khlebnikov, Phys. Rev. D 46 (1992) 3223.
 - [28] P. Arnold, Phys. Rev. D 48 (1993) 1539.
 - [29] G. Moore and T. Prokopec, Phys. Rev. Lett. 75 (1995) 777.

- [30] G.D. Moore and T. Prokopec, PUP-TH-1544 [hep-ph/9506475].
- [31] D. Bödeker, W. Buchmüller, Z. Fodor, and T. Helbig, Nucl. Phys. B 423 (1994) 171.
- [32] K. Kajantie, M. Laine, K. Rummukainen, and M. Shaposhnikov, CERN-TH/95-263 [hep-lat/9510020].
- [33] J.H. Applegate and C.J. Hogan, Phys. Rev. D 31 (1985) 3037.
- [34] G.M. Fuller, G.J. Mathews, and C.R. Alcock, Phys. Rev. D 37 (1988) 1380.
- [35] H. Kurki-Suonio, Phys. Rev. D 37 (1988) 2104.
- [36] K. Sumiyoshi, T. Kajino, C.R. Alcock, and G.J. Mathews, Phys. Rev. D 42 (1990) 3963.
- [37] K. Jedamzik and G.M. Fuller, Nucl. Phys. B 441 (1995) 215.
- [38] K. Jedamzik and G.M. Fuller, Astroph. J. 423 (1994) 33.



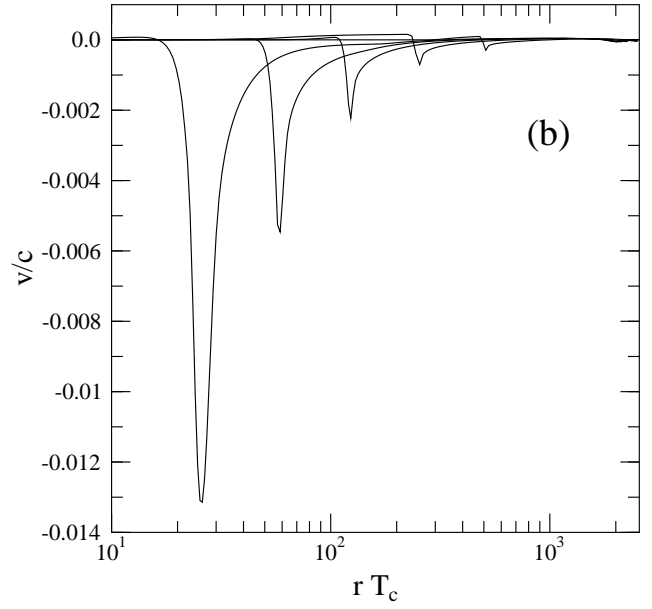
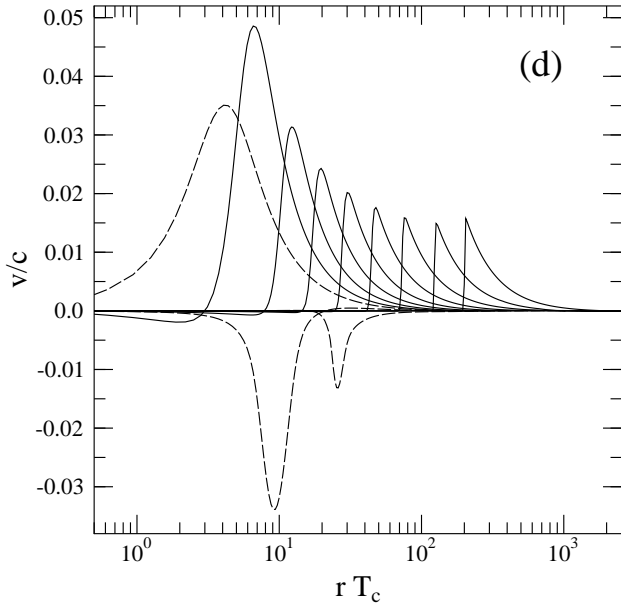
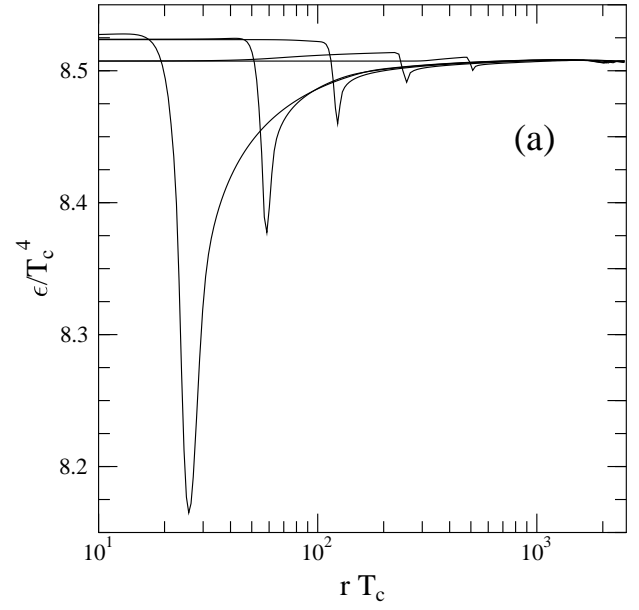
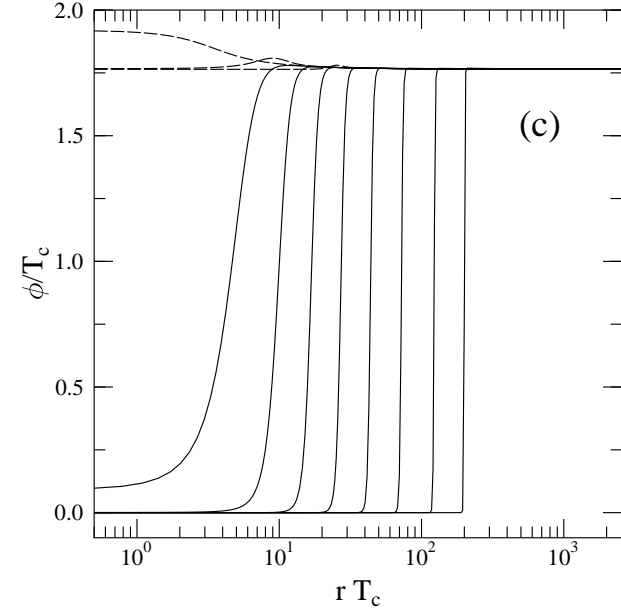


FIG. 7. Results from the run. We show profiles for four quantities: proper energy density (a), local temperature (b), order parameter (c), and flow velocity (d). The solid curves are from successive time-slices as the droplet is shrinking (wall moving to the left). The dashed curves are from time-slices after the droplet has disappeared (pattern moving to the right). We use a logarithmic axis for the radial coordinate to focus on the droplet evaporation site. The finite thickness of the wall becomes thus apparent when the wall has reached small values of r .

FIG. 8. Results from the same run as Fig. 7. We show later time slices (after droplet evaporation) of proper energy density (a) and flow velocity (b) with an expanded scale. A pulse of inward flow is moving outwards and decaying rapidly, evening out the energy density (and other thermodynamic quantities).

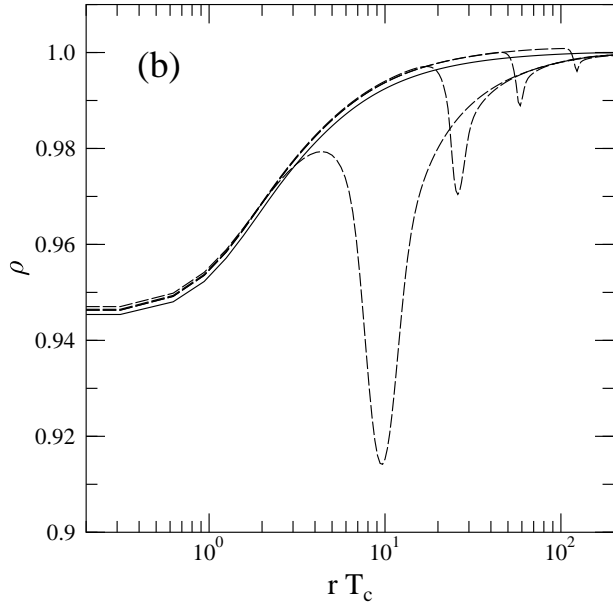
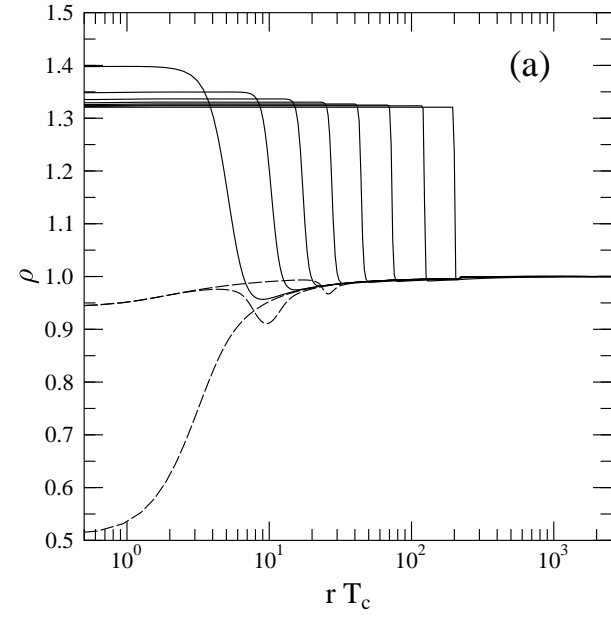


FIG. 9. The compression factor ρ . The upper figure (a) is like Fig. 7. The lower figure (b) is a close-up near the droplet evaporation site and shows time slices after droplet evaporation. The solid line is the final ρ -profile, showing the decompression due to droplet surface energy. Note the very small spatial extension of the decompressed region.

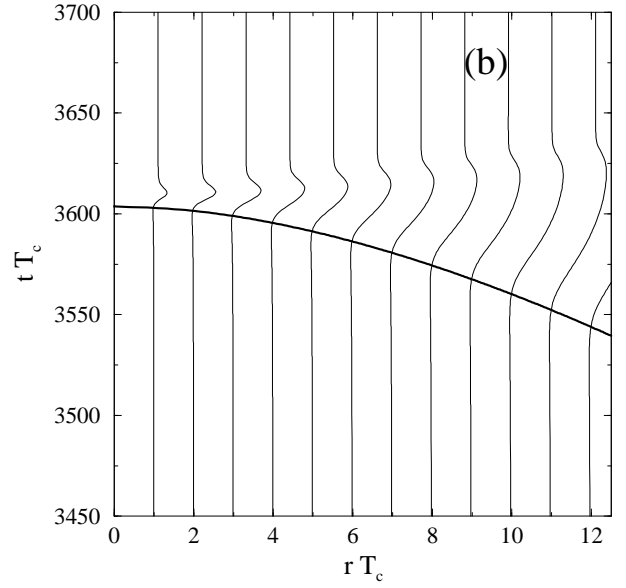
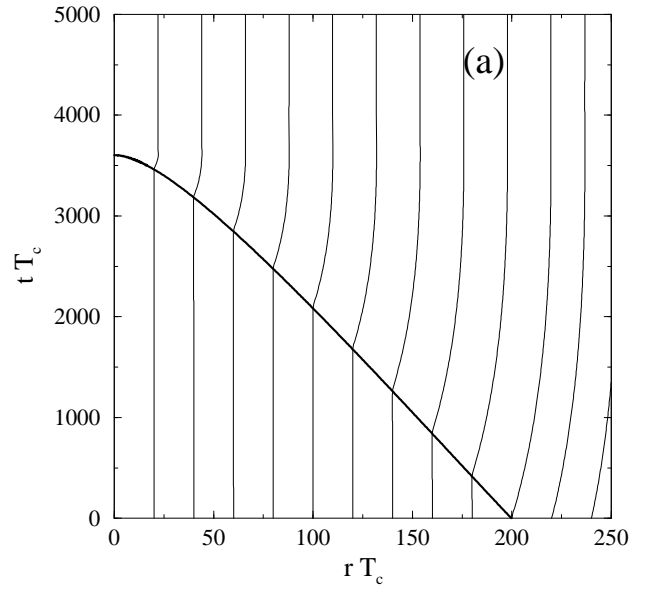


FIG. 10. The flow lines of particles moving with the fluid. The lower figure (b) is a magnification of the final stages. This figure contains the same information as Fig. 9, but in a different form. At the time of the droplet decay, there is a local rarefaction and subsequent compression near the droplet, but no global rarefaction wave is left behind. Due to the difficulty of getting baryon number across the phase transition surface (the thick line), a part of the baryon number would not follow the flow lines but would instead remain in the quark phase.